

Engineered cardiac tissue analyzed using the mechanical bidomain model

Kharananda Sharma and Bradley J. Roth

Department of Physics, Oakland University, Rochester, Michigan 48309-4479, USA



(Received 5 February 2018; revised manuscript received 26 June 2018; published 5 November 2018)

Experiments show that when engineered cardiac tissue is stretched, cells grow preferentially at the free edge of the tissue compared to the interior. In order to understand why cells grow near the edge, the mechanical bidomain model is used to simulate these experiments. This mathematical model of mechanotransduction treats the intra- and extracellular spaces individually, and predicts the force on integrin proteins in the cell membrane. The bidomain equations are solved numerically using the finite-difference method. The simulations predict that the difference between intra- and extracellular displacements, which the model assumes is the driving force behind cellular growth and remodeling, is largest near the free edge of a sheet of tissue, and is smallest at the center, consistent with experiments.

DOI: [10.1103/PhysRevE.98.052402](https://doi.org/10.1103/PhysRevE.98.052402)

I. INTRODUCTION

Mechanotransduction is the mechanism by which mechanical forces cause tissue to grow and remodel. Mechanical forces play a role in growing engineered cardiac tissue [1–8]. Fink *et al.* [9] examined the influence of chronic mechanical stretch in engineered heart tissue (embryonic chick or neonatal rat cardiac myocytes grown in a collagen matrix). The engineered tissue was subjected to a unidirectional stretch for six days in serum-containing medium. A high concentration of cells grew near the free edge of the tissue, but not in the interior (Fig. 1, see arrows).

The mechanical bidomain model is a mathematical model that represents cardiac tissue as a continuum yet accounts for forces acting across the myocardial membrane [10,11]. The central hypothesis of the mechanical bidomain model is that the difference in displacements between intra- and extracellular spaces produce forces on membrane proteins such as integrins which then initiate a cascade of events leading to cell growth and remodeling [12–15]. The transduction of mechanical signals is crucial in many biological contexts from stem cell biology to tissue engineering, and from cancer to development [16].

Most previous mathematical models have focused on tissue stress and strain as causing cardiac tissue growth and remodeling [17–21]. These are monodomain models; they represent the tissue as a single phase. The bidomain model is different than previous monodomain models because it assumes that mechanotransduction is driven not by stress or strain, but instead by differences between intra- and extracellular displacements [11]. One weakness of the bidomain model is that it has not been confirmed experimentally.

In this paper, we use the mechanical bidomain model to simulate the Fink *et al.* [9] experiment. Our goal is to predict tissue strain (a monodomain concept) and the difference in intra- and extracellular displacement (a bidomain concept), and compare these two predictions to determine which provides a better qualitative explanation of the experimental data. In particular, we will determine which concept better explains the preferential cell growth near the free edge of the tissue.

II. METHODS

A. Bidomain equations

In a two-dimensional sheet of linear isotropic tissue under plane strain, the relationships between the stress $\boldsymbol{\tau}$ and strain $\boldsymbol{\epsilon}$ in the intracellular (*i*) and extracellular (*e*) spaces are [11]

$$\begin{aligned} \tau_{ixx} &= -p + 2\nu\epsilon_{ixx}, & \tau_{iyy} &= -p + 2\nu\epsilon_{iyy}, \\ \tau_{ixy} &= 2\nu\epsilon_{ixy}, \end{aligned} \quad (1)$$

$$\begin{aligned} \tau_{exx} &= -q + 2\mu\epsilon_{exx}, & \tau_{eyy} &= -q + 2\mu\epsilon_{eyy}, \\ \tau_{exy} &= 2\mu\epsilon_{exy}. \end{aligned} \quad (2)$$

The parameters ν and μ are the shear moduli of the intra- and extracellular spaces, and p and q are intra- and extracellular hydrostatic pressures. The strains are related to the intra- and extracellular displacements \mathbf{u} and \mathbf{w} by

$$\epsilon_{ixx} = \frac{\partial u_x}{\partial x}, \quad \epsilon_{iyy} = \frac{\partial u_y}{\partial y}, \quad \epsilon_{ixy} = \frac{1}{2} \left(\frac{\partial u_x}{\partial y} + \frac{\partial u_y}{\partial x} \right), \quad (3)$$

$$\epsilon_{exx} = \frac{\partial w_x}{\partial x}, \quad \epsilon_{eyy} = \frac{\partial w_y}{\partial y}, \quad \epsilon_{exy} = \frac{1}{2} \left(\frac{\partial w_x}{\partial y} + \frac{\partial w_y}{\partial x} \right). \quad (4)$$

Biological tissue is mainly composed of water; therefore, the intra- and extracellular spaces are each incompressible, \mathbf{u} and \mathbf{w} have zero divergence, and the displacements can be obtained by differentiating the intra- and extracellular stream functions ϕ and η [10],

$$u_x = \frac{\partial \phi}{\partial y}, \quad u_y = -\frac{\partial \phi}{\partial x} \quad (5)$$

$$w_x = \frac{\partial \eta}{\partial y}, \quad w_y = -\frac{\partial \eta}{\partial x}. \quad (6)$$

Substituting (1)–(6) into the equations of mechanical equilibrium [11], we obtain the equations of the mechanical

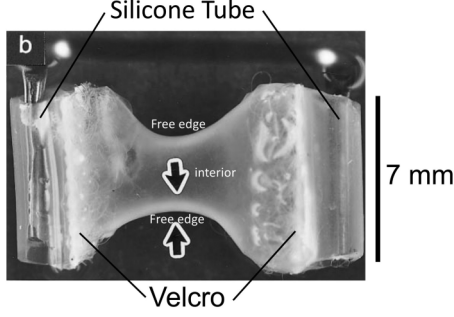


FIG. 1. Photograph of 6-day-stretched engineered cardiac tissue. The silicone tubes stretch the tissue by pulling to the left and right. The large arrows show cells (white) growing preferentially at the free edge. Used with permission from Fink *et al.* [9].

bidomain model [10],

$$-\frac{\partial p}{\partial x} + \nu \left(\frac{\partial^3 \phi}{\partial x^2 \partial y} + \frac{\partial^3 \phi}{\partial y^3} \right) = K \left(\frac{\partial \phi}{\partial y} - \frac{\partial \eta}{\partial y} \right), \quad (7)$$

$$-\frac{\partial q}{\partial x} + \mu \left(\frac{\partial^3 \eta}{\partial x^2 \partial y} + \frac{\partial^3 \eta}{\partial y^3} \right) = -K \left(\frac{\partial \phi}{\partial y} - \frac{\partial \eta}{\partial y} \right), \quad (8)$$

$$-\frac{\partial p}{\partial y} - \nu \left(\frac{\partial^3 \phi}{\partial x \partial y^2} + \frac{\partial^3 \phi}{\partial x^3} \right) = -K \left(\frac{\partial \phi}{\partial x} - \frac{\partial \eta}{\partial x} \right), \quad (9)$$

$$-\frac{\partial q}{\partial y} - \mu \left(\frac{\partial^3 \eta}{\partial x \partial y^2} + \frac{\partial^3 \eta}{\partial x^3} \right) = K \left(\frac{\partial \phi}{\partial x} - \frac{\partial \eta}{\partial x} \right). \quad (10)$$

The parameter K is the spring constant of the integrins coupling the intra- and extracellular spaces. By taking the y derivative of (7) and subtracting the x derivative of (9) we can eliminate the pressure p and get [10]

$$\nu \nabla^4 \phi = K (\nabla^2 \phi - \nabla^2 \eta). \quad (11)$$

Similarly,

$$\mu \nabla^4 \eta = -K (\nabla^2 \phi - \nabla^2 \eta). \quad (12)$$

We can write the bidomain equations in terms of the monodomain and bidomain stream functions ψ and λ instead of the intra- and extracellular stream functions ϕ and η , where

$$\psi = \phi + \frac{\mu}{\nu} \eta, \quad \lambda = \phi - \eta. \quad (13)$$

Furthermore, we can recast the equations in terms of dimensionless parameters

$$X = \frac{x}{D}, \quad Y = \frac{y}{D}, \quad \epsilon = \frac{\mu \nu}{K(\nu + \mu)D^2}, \quad (14)$$

where $2D$ is the length and width of the tissue sheet ($-1 < X, Y < 1$). Writing (11) and (12) in terms of ψ , λ , and the dimensionless parameters yields [10]

$$\nabla^4 \psi = 0, \quad (15)$$

$$\nabla^4 \lambda = \frac{1}{\epsilon} \nabla^2 \lambda, \quad (16)$$

where now the derivatives are with respect to X and Y (Fig. 2).

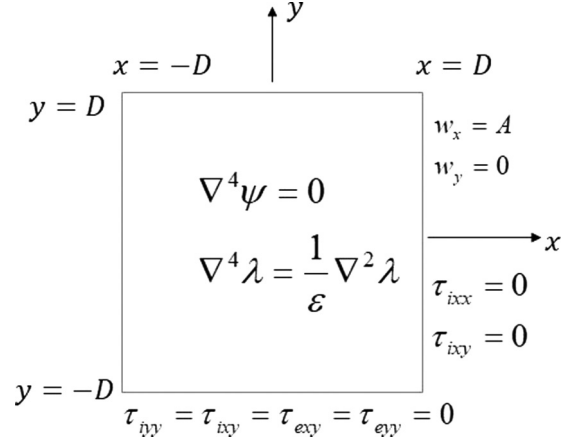


FIG. 2. A sheet of cardiac tissue. The differential equations (15) and (16) govern the monodomain and bidomain stream functions ψ and λ . On the top and bottom, the tissue is free (zero stress). At the left and right, the extracellular displacement is given and the intracellular space is free.

B. Boundary conditions

The behavior of the tissue depends on the boundary conditions, which are different on the left and right surfaces compared to the top and bottom surfaces.

1. Left and right surfaces

At $x = D$, we displace the extracellular space by an amount A to the right, so $w_x = A$ and $w_y = 0$. In terms of the extracellular stream function, these boundary conditions are

$$\frac{\partial \eta}{\partial y} = A, \quad (17)$$

$$\frac{\partial \eta}{\partial x} = 0. \quad (18)$$

We further assume that the intracellular space is free (the force pulling on the tissue is exerted only on the extracellular space), so $\tau_{ixx} = \tau_{ixy} = 0$. The condition $\tau_{ixy} = 0$ implies that

$$\frac{\partial^2 \phi}{\partial y^2} - \frac{\partial^2 \phi}{\partial x^2} = 0. \quad (19)$$

The condition $\tau_{ixx} = 0$ implies that $-p + 2\nu \frac{\partial^2 \phi}{\partial x \partial y} = 0$. One problem is that we do not calculate the pressure. We can, however, take the y derivative of this condition to get $-\frac{\partial p}{\partial y} + 2\nu \frac{\partial^3 \phi}{\partial x \partial y^2} = 0$ [22]. If we use (9) to eliminate $\frac{\partial p}{\partial y}$, we obtain

$$\nu \left(3 \frac{\partial^3 \phi}{\partial x \partial y^2} + \frac{\partial^3 \phi}{\partial x^3} \right) = K \left(\frac{\partial \phi}{\partial x} - \frac{\partial \eta}{\partial x} \right). \quad (20)$$

Next, we express the four boundary conditions (17)–(20) in terms of ψ and λ instead of ϕ and η , and use nondimensional parameters X , Y , and ϵ to find

$$\frac{\partial \psi}{\partial Y} = \frac{\partial \lambda}{\partial Y} + \left(\frac{\nu + \mu}{\nu} \right) AD, \quad (21)$$

$$\frac{\partial \psi}{\partial X} = \frac{\partial \lambda}{\partial X}, \quad (22)$$

$$\frac{\mu}{v} \left(\frac{\partial^2 \lambda}{\partial Y^2} - \frac{\partial^2 \lambda}{\partial X^2} \right) = - \left(\frac{\partial^2 \psi}{\partial Y^2} - \frac{\partial^2 \psi}{\partial X^2} \right), \quad (23)$$

$$\frac{\mu}{v} \left(3 \frac{\partial^3 \lambda}{\partial X \partial Y^2} + \frac{\partial^3 \lambda}{\partial X^3} - \frac{1}{\epsilon} \frac{\partial \lambda}{\partial X} \right) = - \left(3 \frac{\partial^3 \psi}{\partial X \partial Y^2} + \frac{\partial^3 \psi}{\partial X^3} \right). \quad (24)$$

At $x = -D$, the boundary conditions are the same except $\frac{\partial \eta}{\partial y} = -A$ (the tissue is pulled to the left).

2. Top and bottom surfaces

At $y = \pm D$ the surface is free, so $\tau_{iyy} = \tau_{ixy} = \tau_{eyy} = \tau_{exy} = 0$. Following similar methods as for the left and right surfaces, we get the boundary conditions

$$3 \frac{\partial^3 \lambda}{\partial X^2 \partial Y} + \frac{\partial^3 \lambda}{\partial Y^3} - \frac{1}{\epsilon} \frac{\partial \lambda}{\partial Y} = 0, \quad (25)$$

$$3 \frac{\partial^3 \psi}{\partial X^2 \partial Y} + \frac{\partial^3 \psi}{\partial Y^3} = 0, \quad (26)$$

$$\frac{\partial^2 \lambda}{\partial Y^2} - \frac{\partial^2 \lambda}{\partial X^2} = 0, \quad (27)$$

$$\frac{\partial^2 \psi}{\partial Y^2} - \frac{\partial^2 \psi}{\partial X^2} = 0. \quad (28)$$

C. Numerical methods

We use the finite-difference approximation to solve the bidomain equations [23,24]. We replace the derivatives by finite differences and solve the resulting difference equations by successive overrelaxation, with the overrelaxation parameter $W = 1.4$ and a total of 10^6 iterations. The boundary conditions (21)–(28) are implemented using two phantom nodes at each boundary. We can reduce the computation time by calculating over only one quadrant of the sheet; the behavior of the other three quadrants is found from symmetry. In one quadrant the tissue is represented by an $N \times N$ grid, where N is the number of nodes in each direction. The entire tissue ranges from $-D < x, y < D$, so one quadrant ranges from $0 < x, y < D$. The space step is therefore $\Delta = \frac{D}{(N-1)}$. We use $N = 41$ (not including the phantom nodes) so $\Delta = \frac{D}{40}$. We assume that $v = \mu$ and $\epsilon = 0.000625$. This value of ϵ implies that the bidomain length constant $\sigma = \sqrt{\frac{v\mu}{K(v+\mu)}}$ [11] is equal to $\frac{D}{40}$, the same as the space step. To match the Fink *et al.* [9] experiment, we take $D = 5$ mm and $A = 1$ mm, implying $\Delta = \sigma = 0.125$ mm.

Additional details about the calculations and the MATLAB code can be found in Ref. [25].

III. RESULTS

Let us define monodomain and bidomain displacements \mathbf{m} and \mathbf{b} such that

$$m_x = \frac{\partial \psi}{\partial y}, \quad m_y = -\frac{\partial \psi}{\partial x}, \quad b_x = \frac{\partial \lambda}{\partial y}, \quad b_y = -\frac{\partial \lambda}{\partial x}. \quad (29)$$

The monodomain displacement \mathbf{m} represents the behavior that would be predicted if the tissue were represented as a single phase with shear modulus $v + \mu$, rather than representing the intracellular and extracellular spaces as two coupled

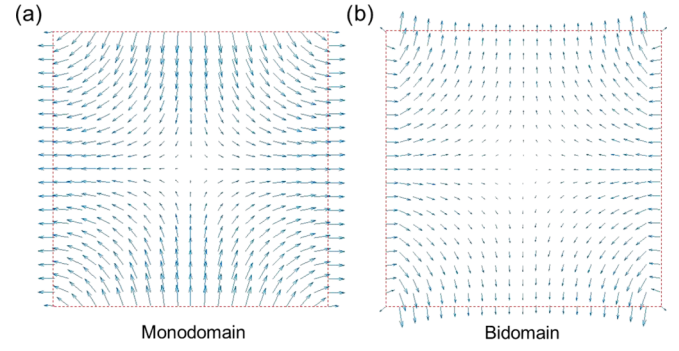


FIG. 3. (a) The monodomain displacement \mathbf{m} , and (b) the bidomain displacement \mathbf{b} , as functions of position. The red dashed box indicates the boundary of the sheet. The tissue is stretched on the left and right edges and is free on the top and bottom edges. The vectors are not drawn to scale. $v = \mu$, $\epsilon = 0.000625$, $A = 1$ mm, and $D = 5$ mm.

phases. Most biomechanical models are monodomain models. Figure 3(a) shows the distribution of \mathbf{m} . Because the tissue is incompressible, the top and bottom edges move inward as the left and right sides are pulled outward. All figures use symmetry to show all four quadrants, even though the calculation was performed in only one quadrant.

The bidomain displacement \mathbf{b} describes the difference between the intracellular and extracellular displacements. Our hypothesis is that mechanotransduction is driven by the bidomain displacement. Figure 3(b) plots the distribution of \mathbf{b} .

The monodomain displacement is much larger than the bidomain displacement; the arrows in the plots of Figs. 3(a) and 3(b) use different scales. If plotted on the same scale, the largest bidomain arrows near the tissue corners would be about 15 times smaller than the largest monodomain arrows, and at the center of the free edge ($x = 0, y = D$) the bidomain arrows are 47 times smaller than the monodomain arrows. The monodomain displacement is relatively insensitive to ϵ , but the bidomain displacement \mathbf{b} depends sensitively on ϵ . When we compare the monodomain displacement $|\mathbf{m}|$ using $\epsilon = 0.000625$ and 0.00625 , its peak value changes by a factor of 0.89 (11% decrease), whereas the peak value of $|\mathbf{b}|$ changes by a factor of 2.62 (162% increase). The bidomain displacement varies over a short distance near the left and right edges (note how the y component of \mathbf{b} changes sign at the edge). This behavior is particularly noticeable near the corners of the sheet. The monodomain behavior, on the other hand, is much smoother.

In the bidomain model, the difference between intra- and extracellular displacements, $\mathbf{b} = \mathbf{u} - \mathbf{w}$, drives mechanotransduction, and is therefore the central quantity. Figure 4 represents the magnitude of the bidomain displacement $|\mathbf{b}|$. It is zero at the center of the tissue and is increasingly larger toward the edges. It is largest near the corners, but has a significant value all along the free edge (arrows). This result implies that mechanotransduction should be smallest at the tissue center, and larger near the edges.

Figure 5 shows the monodomain strains: Fig. 5(a) is the normal strain ϵ_{ixx} and Fig. 5(b) is the shear strain ϵ_{ixy} . The strains are distributed throughout the tissue. The shear strain is

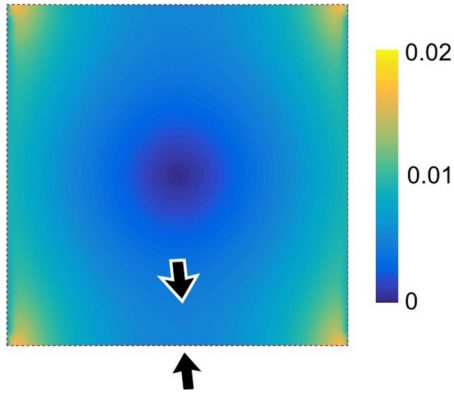


FIG. 4. The magnitude of the difference in displacements between intra- and extracellular spaces, $|\mathbf{b}|$. The arrows show $|\mathbf{b}|$ is significant near the free top and bottom edges. The dashed box indicates the edge of the sheet. $\nu = \mu$ and $\epsilon = 0.000\,625$, $A = 1$ mm, and $D = 5$ mm.

localized near the corners, but the normal strain is large at the tissue center and smaller on the edges. The distribution of the bidomain displacement $|\mathbf{b}|$ (Fig. 4) is qualitatively different than the distribution of strains (Fig. 5), so the prediction of where cells grow depends on if $|\mathbf{b}|$ or strain drives mechanotransduction.

IV. DISCUSSION

Our calculation provides a theoretical explanation for the distribution of cell growth of engineered heart tissue observed in experiments [9,26]. In particular, when a sheet of engineered tissue is stretched, cells grow preferentially near the free edge (Fig. 1). The mechanical bidomain model predicts similar behavior: Mechanotransduction—which the model assumes is caused by differences between the intracellular and extracellular displacements, or $|\mathbf{b}|$ —is larger near the free edge of the sheet compared with the center (Fig. 4). Although our model may not predict the quantitative distribution of cell growth observed experimentally, it does reproduce the qualitative localization of cell growth near the tissue edge.

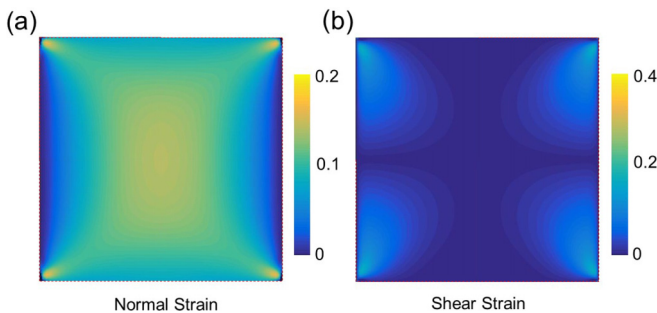


FIG. 5. (a) The intracellular normal strain ϵ_{ixx} and (b) the intracellular shear strain ϵ_{ixy} . $\nu = \mu$, $\epsilon = 0.000\,625$, $A = 1$ mm, and $D = 5$ mm. The shear strain is actually an odd function of x and y , but we assume mechanotransduction would depend on the magnitude but not the sign of ϵ_{ixy} , so we plot its absolute value in (b). The Pearson correlation coefficient between the data in Fig. 4 and (a) is -0.6137 , and between Fig. 4 and (b) is 0.6256 .

If strain were responsible for tissue growth, as is assumed in monodomain models [17–21], then the model indicates that growth should be larger in the center than near the edge (Fig. 5).

Our calculation is performed in nondimensional coordinates X and Y . Assume that $D = 5$ mm, which is roughly the size of Fink *et al.*'s engineered tissue constructs. In that case, the space step Δ and the bidomain length constant σ are both $125\ \mu\text{m}$. Experiments on colonies of growing embryonic stem cells indicate that σ is on the order of $150\ \mu\text{m}$ [27,28] but σ may be smaller in cardiac tissue *in vivo*. Previous bidomain calculations indicate that there is a boundary layer near the tissue edge that has a thickness σ [11]. We observe such a boundary layer near the edge of tissue that is stretched [Fig. 3(b)]. This behavior is difficult to compare to the experimental data (Fig. 1) because in the experiment Velcro is used to make contact with a silicone tube that exerts the force to stretch the tissue, obscuring edge effects there. Interestingly, the cell growth occurring at the free boundary does not fall off with the length constant. The cell growth extends far into the tissue (but not to the center), qualitatively consistent with experiments (Fig. 1). In our calculations, making σ smaller requires a smaller space step, implying a larger value of N and even more iterations, slowing the calculation dramatically. Finite-element calculations, such as those used by Sharma *et al.* [11], would allow us to use a finer space step near the edge and especially near the corner.

The peak value of $|\mathbf{b}|$ in Fig. 4 is on the order of $200\ \mu\text{m}$, which seems too large. Several reasons may explain this. (1) The displacements at the corners are unreasonably large. The experimental tissue sample used by Fink *et al.* [9] does not have such sharp corners that concentrate the stress and displacement. (2) Our value of σ , $125\ \mu\text{m}$, is probably too large. (3) Integrins have a large extracellular region that extends far into the extracellular space [29], implying that $|\mathbf{b}|$ may be larger than we might expect. (4) The macroscopic bidomain displacement \mathbf{b} may be different than the microscopic displacement at the integrin because of microscopic displacements of the intra- and extracellular spaces around the protein. (5) The force-displacement relationship of the integrin may in fact be nonlinear, suppressing the largest values of \mathbf{b} . The absolute value of \mathbf{b} in Fig. 4 depends strongly on the value of σ and therefore ϵ , but the spatial distribution of \mathbf{b} depends weakly on ϵ .

Is mechanotransduction the mechanism for cell growth at the boundary? Fink *et al.* [9] observe this effect in stretched tissue more than in unstretched controls, suggesting it is related to mechanotransduction. It does not appear to be an issue of oxygen or nutrients having difficulty diffusing into the tissue, because Fink *et al.* [9] use thin tissue sheets. Zimmermann *et al.* [1] suggest that “the cell gradient from the edges to the center is most likely due to load differences between the edges and the center of the matrix.” We would argue that our model predicts mathematically what Zimmerman *et al.* [1] mean by their qualitative statement, and it is not the “load” but “ $|\mathbf{b}|$ ” that is different between the edges and the center.

Our calculation has several limitations:

(a) The mechanical bidomain model is macroscopic, in that it represents the tissue averaged over many cells. While

this may capture large-scale behavior, microscopic properties at the cellular or even molecular level may also contribute to the behavior [30–33]. In the electrical bidomain model [34], the relationship between the microscopic and macroscopic behavior has been analyzed rigorously [35]. A similar analysis has not been performed for the mechanical bidomain model.

(b) We assume a linear strain and linear stress-strain relationships in the intra- and extracellular spaces. However, the strains applied by Fink *et al.* [9] are about 20%, so that a linear strain is a reasonable first approximation, but there could be a significant effect from nonlinearities.

(c) We assume the tissue is isotropic. Fink *et al.* [9] observe that near the free edges, the cell shape has a more anisotropic appearance than near the center. The assumption of isotropy may be only an approximation and the tissue may become more anisotropic over time [30,31]. Additional analysis is needed to quantify the role of anisotropy in these studies. The condition of “unequal anisotropy ratios” plays a key role in the electrical bidomain model [34], and differences between the anisotropy of the intra- and extracellular spaces may likewise be important for the mechanical bidomain model.

(d) A complete analysis would represent the tissue sheet as three dimensional. However, the tissue constructs created by Fink *et al.* had dimensions of about $0.18 \times 8 \times 15$ mm [26]. Because their length and width were approximately 50 times their thickness, as a first approximation we treated the tissue sheet as being two dimensional.

(e) We assume the integrin spring is linear, isotropic, and Hookean. It may, in fact, be nonlinear.

(f) We assume plane strain, where there are no displacements or strains in the direction perpendicular to the tissue sheet (z). An alternative approach would be to model the tissue using plane stress [27,36].

(g) We only analyze the steady-state mechanical response. Fink *et al.* [9] apply a sinusoidal stretching with a frequency of about 1.5 Hz. Viscoelastic behavior [37] would not be captured by our calculations. However, viscoelasticity should primarily affect the temporal response of the tissue, whereas our study focuses on the spatial distribution of the response.

(h) We assume that each space in the tissue is incompressible. This will be a good assumption as long as the applied stretching is at a high enough frequency that there is not significant water movement in one period. If water movement does occur, the incompressible assumption may be violated and water may be squeezed out of the tissue as in a sponge.

(i) We assume a square tissue sheet. In fact, the tissue is biconcave with a narrower width near the center than at the edges (Fig. 1). Our model predicts such a geometry when stretched, but if the tissue grows so that it has this shape when not stretched, our simple tissue geometry may not capture the full behavior.

(j) On the left and right sides of the tissue, we assume the extracellular space is stretched but the intracellular space has zero stress. This assumption is consistent with our previous studies [11], and implies that whatever force is stretching the tissue acts on the extracellular matrix; the only reason the intracellular space displaces is because it is pulled by integrins. A similar issue of boundary conditions arises in the electrical bidomain model [38].

Despite these limitations, the mechanical bidomain model does predict a remarkable property of these engineered sheets of cardiac tissue: the preferential growth of cells near the free surface relative to the center. A key prediction of the model is that the difference in displacement (a bidomain quantity) has a different distribution than the strain (a monodomain quantity). The location where cells grow depends on if the difference in displacement or strain drives mechanotransduction. Our results, plus the study of stem cell differentiation in cell colonies [27], highlight experimental evidence supporting the bidomain model over the monodomain model for describing mechanotransduction.

ACKNOWLEDGMENTS

This work was funded by the King-Chavez-Parks Future Faculty Fellowship Program, State of Michigan.

The authors declare that they have no conflict of interest.

-
- [1] W. H. Zimmermann, I. Melnychenko, and T. Eschenhagen, Engineered heart tissue for regeneration of diseased hearts, *Biomaterials* **25**, 1639 (2004).
 - [2] L. D. Butler, A. S. Goldstein, E. R. Guldborg, X. E. Guo, R. Kamm, T. C. Laurencin, V. L. McIntire, C. V. Mow, M. R. Nerem, L. R. Sah, J. L. Soslowsky, L. R. Spilker, and T. R. Tranquillo, The impact of biomechanics in tissue engineering and regenerative medicine, *Tissue Eng., Part B* **15**, 1089 (2009).
 - [3] G. Vunjak-Novakovic, N. Tandon, A. Godier, R. Maidhof, A. Marsano, P. T. Martens, and M. Radisic, Challenges in cardiac tissue engineering, *Tissue Eng., Part B* **16**, 169 (2010).
 - [4] N. M. Hirt, A. Hansen, and T. Eschenhagen, Cardiac tissue engineering, *Circ. Res.* **114**, 354 (2014).
 - [5] K. Kroll, M. Chabria, K. Wang, F. Hausermann, F. Schuler, and L. Polonchuk, Electro-mechanical conditioning of human iPSC-derived cardiomyocytes for translational research, *Prog. Biophys. Mol. Biol.* **130**, 212 (2017).
 - [6] A. Koroli, E. Y. Wang, R. A. Civitarese, and M. Radisic, Biophysical stimulation for *in vitro* engineering of functional cardiac tissues, *Clin. Sci.* **131**, 1393 (2017).
 - [7] F. Weinberger, I. Mannhavdt, and T. Eschenhagen, Engineering cardiac muscle tissue: A maturing field of research, *Circ. Res.* **120**, 1487 (2017).
 - [8] K. Y. Morgan and L. D. Black, Investigation into the effects of varying frequency of mechanical stimulation in a cycle-by-cycle manner on engineered cardiac construct function, *J. Tissue Eng. Regener. Med.* **11**, 342 (2017).
 - [9] C. Fink, S. Ergün, D. Kralisch, U. Remmers, J. Weil, and T. Eschenhagen, Chronic stretch of engineered heart tissue induces hypertrophy and functional improvement, *FASEB J.* **14**, 669 (2000).
 - [10] B. J. Roth, The mechanical bidomain model: A review, *ISRN Tissue Eng.* **2013**, 863689 (2013).

- [11] K. Sharma, N. Al-asuoad, M. Shillor, and B. J. Roth, Intracellular, extracellular, and membrane forces in remodeling and mechanotransduction: The mechanical bidomain model, *J. Coupled Syst. Multiscale Dyn.* **3**, 200 (2015).
- [12] B. E. Dabiri, H. Lee, and K. K. Parker, A potential role for integrin signaling in mechano-electrical feedback, *Prog. Biophys. Mol. Biol.* **110**, 196 (2012).
- [13] R. K. Harston and D. Kuppaswamy, Integrins are the necessary links to hypertrophic growth in cardiomyocytes, *J. Signal Transduct.* **2011**, 521742.
- [14] R. Janostiak, A. Csilla Pataki, J. Brabek, and D. Rosel, Mechanosensors in integrin signaling: The emerging role of p130Cas, *Eur. J. Cell Biol.* **93**, 445 (2014).
- [15] W. L. Stoppel, D. L. Kaplan, and L. D. Black III, Electrical and mechanical stimulation of cardiac cells and tissue constructs, *Adv. Drug Delivery Rev.* **96**, 135 (2016).
- [16] C. R. Jacobs, H. Huang, and R. Y. Kwon, *Introduction to Cell Mechanics and Mechanobiology* (Garland, New York, 2013).
- [17] W. Kroon, T. Delhaas, P. Bovendeerd, and T. Arts, Computational analysis of the myocardial structure: Adaptation of cardiac myofiber orientations through deformation, *Med. Image Anal.* **13**, 346 (2009).
- [18] R. C. P. Kerckhoffs, Computational modeling of cardiac growth in post-natal rat with a strain-based growth law, *J. Biomech.* **45**, 865 (2012).
- [19] R. C. P. Kerckhoffs, J. H. Omens, and A. D. McCulloch, A single strain-based growth law predicts concentric and eccentric cardiac growth during pressure and volume overload, *Mech. Res. Commun.* **42**, 40 (2012).
- [20] P. H. M. Bovendeerd, Modeling of cardiac growth and remodeling of myofiber orientation, *J. Biomech.* **45**, 872 (2012).
- [21] L. C. Lee, G. S. Kassab, and J. M. Guccione, Mathematical modeling of cardiac growth and remodeling, *WIREs Syst. Biol. Med.* **8**, 211 (2016).
- [22] M. Mitchel, Exact and numerical solution for Stokes flow in glaciers, Thesis, University of Alaska Fairbanks, 2012.
- [23] S. P. Gandhi and B. J. Roth, A numerical solution of the mechanical bidomain model, *Comput. Methods Biomech. Biomed. Eng.* **19**, 1099 (2016).
- [24] K. Sharma and B. J. Roth, A multiscale mechanical bidomain model of cardiac tissue with complex fiber geometry, in *5th International Conference on Computational and Mathematical Biomedical Engineering*, April 10–12, 2017, Pittsburgh, Pennsylvania, edited by P. Nithiarasu *et al.* (CMBE, Swansea, U.K., 2017), Vol. 1, p. 468.
- [25] K. Sharma, The mechanical bidomain model of cardiac tissue, Dissertation, Oakland University, Rochester, MI, 2018.
- [26] T. Eschenhagen, C. Fink, U. Remmers, H. Scholz, J. Wattchow, J. Weil, W. Zimmermann, H. H. Dohmen, H. Schäfer, T. Wakatsuki, and L. E. Elson, Three-dimensional reconstitution of embryonic cardiomyocytes in a collagen matrix: A new heart muscle model system, *FASEB J.* **11**, 683 (1997).
- [27] D. Auddya and B. J. Roth, A mathematical description of a growing cell colony based on the mechanical bidomain model, *J. Phys. D* **50**, 105401 (2017).
- [28] K. A. Rosowski, A. F. Mertz, S. Norcross, E. R. Dufresne, and V. Horsley, Edges of human embryonic stem cell colonies display distinct mechanical properties and differentiation potential, *Sci. Rep.* **5**, 14218 (2015).
- [29] B.-H. Luo, C. V. Carman, and T. A. Springer, Structural basis of integrin regulation and signaling, *Annu. Rev. Immunol.* **25**, 619 (2007).
- [30] G.-K. Xu, B. Li, X.-Q. Feng, and A. Gao, A tensegrity model of cell reorientation on cyclically stretched substrates, *Biophys. J.* **111**, 1478 (2016).
- [31] G.-K. Xu, X.-Q. Feng, and H. Gao, Orientations of cells on compliant substrates under biaxial stretches: A theoretical study, *Biophys. J.* **114**, 701 (2018).
- [32] G.-K. Xu, J. Qian, and J. Hu, The glycocalyx promotes cooperative binding and clustering of adhesion receptors, *Soft Matter* **12**, 4572 (2016).
- [33] G.-K. Xu, J. Hu, R. Lipowsky, and T. R. Weikl, Binding constants of membrane-anchored receptors and ligands: A general theory corroborated by Monte Carlo simulations, *J. Chem. Phys.* **143**, 243136 (2015).
- [34] C. S. Henriquez, Simulating the electrical behavior of cardiac tissue using the bidomain model, *Crit. Rev. Biomed. Eng.* **21**, 1 (1993).
- [35] J. C. Neu and W. Krassowska, Homogenization of syncytial tissues, *Crit. Rev. Biomed. Eng.* **21**, 137 (1993).
- [36] C. Scribner and B. J. Roth, Plane strain versus plane stress in the mechanical bidomain model, Meeting of Minds XXV **25**, 492 (2017).
- [37] J. D. Humphrey, Continuum biomechanics of soft biological tissue, *Proc. R. Soc. London, Ser. A* **459**, 3 (2003).
- [38] W. Krassowska and J. C. Neu, Effective boundary conditions for syncytial tissues, *IEEE Trans. Biomed. Eng.* **41**, 143 (1994).